Applied Surface Science 580 (2022) 152299

Contents lists available at ScienceDirect

Applied Surface Science

journal homepage: www.elsevier.com/locate/apsusc

Full Length Article

Environmental effects on superlubricity of hydrogenated diamond-like carbon: Understanding tribochemical kinetics in O_2 and H_2O environments

Seokhoon Jang, Zhe Chen, Seong H. Kim *

Department of Chemical Engineering and Materials Research Institute, Pennsylvania State University, University Park, PA 16802, United States

ARTICLE INFO

Keywords:
Hydrogenated diamond-like carbon
Superlubricity
Run-in behavior
Tribochemical kinetics
Re-oxidation probability
Removal probability

ABSTRACT

Hydrogenated diamond-like carbon (H-DLC) exhibits superlubricity in inert conditions, making it ideal for protective coating in machines, but its superlubricity is often lost in humid air. Knowing reaction mechanisms of such oxidation processes would be a prerequisite to incorporate environment tolerance into the H-DLC chemistry for superlubricious performance in ambient air. But mechanistic understanding has been hampered by air-oxidation of the tribo-tested H-DLC surface during the sample transfer for ex-situ analyses. As an alternative approach, this study derived a Langmuir-type kinetics model to analyze tribochemical processes occurring at the H-DLC surface in oxidative environments. The model unveiled very distinct environmental effects of O_2 and H_2O on tribochemistry of H-DLC. The O_2-oxidized H-DLC surface retains low friction after the run-in period ($\mu \approx 0.057$) but is susceptible to frictional wear (wear rate $\approx 32\ \mu m^3/(N{\cdot}mm)$). In contrast, the H_2O-oxidized surface is susceptible to the adsorption of water which acts like boundary lubricant layers protecting the surface from wear ($\sim 3.4\ \mu m^3/(N{\cdot}mm)$) but with relatively high friction after the run-in period ($\mu \approx 0.22$). The oxidation probability of H-DLC by O_2 or H_2O ($\sim 10^{-4}$ Torr^{-1} s^{-1}) is found to be comparable to the reaction probability of hydrocarbons on catalytically-active metals ($\sim 10^{-3}$ Torr^{-1} s^{-1}).

1. Introduction

Among various allotropes of carbon, diamond-like carbon (DLC) exhibits excellent mechanical properties and processibility that make it ideal for protective coatings for various engineering applications ranging from cutting tools to automobile parts [1,2]. Especially, a highly-hydrogenated DLC, hereafter called H-DLC, is well known for 'superlubricity' in inert environments such as vacuum or dry nitrogen [2]. In such conditions, they exhibit a coefficient of friction (COF) as small as ≤ 0.01 after a brief run-in period during which COF is initially high (>0.2) and gradually decreasing [3,4]. The superlubricity is desirable for reduction and prevention of parasitic energy loss (friction) and material loss (wear) at the sliding interface of engineering systems. Unfortunately, the superlubricity of the H-DLC films is lost in ambient air [5–7]. This phenomenon is collectively called 'environmental effect' and believed due to the oxidation of H-DLC surfaces by oxygen and water molecules in air [5–7].

To overcome or mitigate the environmental effect, it is important to fully understand mechanisms and kinetics of the surface oxidation process of H-DLC caused by oxygen gas and water vapor in the environment. There have been many attempts to determine the surface chemistry of H-DLC after tribo-testing in inert and oxidative gases [7–10]. However, such *ex-situ* analyses using x-ray photoelectron spectroscopy (XPS) and Raman spectroscopy could not provide definitive insights needed for mechanistic understanding because the surface chemistry of H-DLC can be altered even with a short period of exposure to air [6,11–13]. Therefore, chemical analysis results of the air-exposed samples are often convoluted due to secondary oxidation during the sample transfer from the tribo-testing unit to the designated analytical instrument. Unless the sample is transferred in a completely inert condition, such complications are inevitable in the post-testing chemical analysis [12].

This impediment could be avoided if chemical analysis is done *in situ* during tribo-testing. For that purpose, *in-situ* Raman spectroscopy has been employed and found the formation of graphitic or sp^2-rich transfer film on counter surfaces during the run-in period [3,14,15]. It was also shown that the structure and uniformity of the transfer film play more important roles in determining the COF than its absolute thickness [3]. However, the recorded Raman signal is an average of all signals of the materials within the penetration depth of the probe beam which

* Corresponding author.
E-mail address: shk10@psu.edu (S.H. Kim).

https://doi.org/10.1016/j.apsusc.2021.152299
Received 8 October 2021; Received in revised form 9 December 2021; Accepted 20 December 2021
Available online 22 December 2021

encompasses the entire thickness of the transfer film and the sub-surface region of the substrate as well; thus, the chemical information of the shear plane could not be fully elucidated. Another *in-situ* study employing electron energy loss spectroscopy with transmission electron microscopy (TEM) showed a friction-induced structural transition leading to an increase in the sp^2-hybridized bond fraction at the sliding interface [16]. Unfortunately, *in-situ* TEM study must be done in ultra-high vacuum condition [17] and cannot provide critical insights into the chemistry relevant to the environmental effect.

Friction force cannot explicitly provide surface chemistry information; nonetheless, it can be a useful tool to implicitly probe chemical conditions of the interface during sliding [4,12,18–20]. Although theoretical understanding of quantitative correlation between COF and surface chemistry is still incomplete [21,22], empirical relationships can be used as a means to assess surface conditions under dynamic interfacial shear in environmental conditions. In previous studies, the adsorption isotherm described by the Elovich equation was used to consider the oxidation process of DLC surfaces during the interfacial shear cycles and describe the experimentally-measured COF as a function of sliding speed (i.e. the time exposed to the environment between consecutive cycles) [23–25]. Although this model could fit the experimental data reasonably well, the fitting parameters could not be directly related to specific kinetic processes such as oxidation probability or rate constant. That is because the Elovich equation is purely empirical without relevance to specific physical or reaction mechanisms [26,27]. In another study, the Langmuir adsorption isotherm was employed to describe the steady-state COF of H-DLC in humid conditions [28,29]; but, since the surface oxidation process is continuous throughout the transient run-in and the steady state [12,30], it is kinetically important to describe the COF transition in the run-in period as well as in the steady state. Moreover, since the environmental effect was assumed to be purely due to physisorption and desorption of molecular water species, the previous model could not explain the oxidation reaction of the surface layer and the frictional removal of the oxidation products [28,29].

In this paper, we investigated the run-in and steady-state friction of H-DLC in oxidative environments through a kinetics modeling. To differentiate the effects of oxygen and water, we studied those two conditions separately. It is known that the surface oxidation of H-DLC occurs readily and the growth of the oxidized layer is self-limiting (i.e. its thickness stops at ~ 2 nm) [11,13,31]; this behavior is somewhat similar to the characteristics of the Langmuir surface reaction kinetics describing the growth of surface reaction species up to the saturation coverage and then no more growth [32–34]. For that reason, the Langmuir kinetics was adapted to describe the re-oxidation of the H-DLC surface freshly exposed by wear of the oxidation reaction product via interfacial friction. Analyzing the reciprocating cycle dependence of COF as a function of O_2 and H_2O partial pressure in dry N_2 with this Langmuir-type kinetics revealed distinct tribochemical effects of oxygen and water on the superlubricity of H-DLC.

2. Experimental details

2.1. Preparation of H-DLC films

H-DLC films were deposited on Si(1 0 0) wafers by a plasma-enhanced chemical vapor deposition (PECVD) process, which was fully described in earlier works [1]. In brief, the procedure started with sputtering of the substrate in an argon plasma to remove contaminants on the substrate, followed by deposition of ~ 100 nm-thick silicon as a bonding layer, and then exposing to a plasma produced with 25% CH_4 and 75% H_2 at a self-bias voltage of −500 V to synthesize a 1 μm-thick H-DLC film. The hydrogen content of the produced H-DLC film was about 40 atomic-% [35–37]. The produced H-DLC film was stored in ambient air.

2.2. Reciprocating ball-on-flat tribo-testing

All friction tests were carried out with a custom-made ball-on-flat reciprocating tribometer equipped with a continuous gas flow cell. Before the tribo-test, the H-DLC substrate was cleaned with ethanol first, deionized water next, and finally blow-dried with nitrogen [38]. Bearing balls made of 440C stainless steel (SS) with a diameter of 3 mm and a root-mean-square (RMS) surface roughness of ~ 10 nm were used as a counter-surface [39]. The H-DLC substrate was translated in a bi-directional reciprocating motion at a sliding speed of 3 mm/s over a span of 2.5 mm while it was in contact with the SS ball at an applied normal load of 2 N. Based on the extended Hertzian contact theory for coated substrates [39–42], and the modulus of H-DLC [39], the average contact pressure, contact radius, and deformation depth of the H-DLC surface were estimated to be 703 MPa, 30 μm, and 603 nm, respectively. The contact pressure is about one order of magnitude lower than the hardness (~7 GPa) of pristine H-DLC surface [39,43]. The frictional force exerted to the ball by the reciprocating sliding motion of the substrate was recorded with a strain gauge sensor. The sensor was calibrated by loading known weights and measuring the corresponding voltages. The COF was calculated following the Amontons' law [44–46]. The wear tracks on the H-DLC surface were analyzed with optical profilometry using a Zygo NewView 7300 instrument. The reproducibility of all COFs was checked and confirmed by repeating of friction tests at least three times in each environmental condition.

A gas stream with a desired partial pressure of oxygen and water was flown continuously over the sample in the environmental cell during the entire duration of friction test. An ultrahigh purity nitrogen gas (zero-grade, $H_2O < 3$ ppm, $O_2 < 4$ ppm; based on the supplier's specification) was used as a carrier gas with a flow rate of 2 L/min to maintain the inert environment. The dry oxygen gas environment was prepared by mixing the inert nitrogen gas stream with an ultrahigh purity oxygen gas (UHP-grade, purity > 99.994%; based on the supplier's specification) at a pre-determined ratio. The humid conditions were produced by mixing the dry nitrogen stream with another nitrogen gas stream saturated with water vapor at room temperature at a pre-determined ratio [47]. All experiments were carried out at ambient pressure (≈760 Torr).

2.3. Hydrophilicity of wear track on H-DLC

Although XPS analysis could probe changes in relative functional groups averaged over the probe depth [11,12,48–50], it cannot provide the chemical information of the topmost surface because its probe depth is larger than the thickness of the oxidized layer formed during the tribo-test, which could be further altered by the air exposure after the test [6,12]. Also, it is difficult, although possible through chemical derivatization [11,51,52], to distinguish hydroxyl (C-OH) versus ether (C-O-C) groups in XPS. As an alternative means to probe the difference in chemistry at the topmost surface of the wear track, we tested if the water condensation and wetting behaviors of the wear track vary depending on the environmental condition during the friction test. Immediately after the friction test, the sample was transferred to an optical microscope and cooled with a Peltier cell to ~ 8 °C below the room temperature under the nitrogen stream saturated with water vapor and imaged continuously to monitor water condensation on it. Separate samples were produced with a large wear zone (roughly 4 mm × 4 mm) in controlled environments and water contact angles on the friction-tested area were measured with a ramé-hart Model 295 automated goniometer/ tensiometer. Note that during the transfer of samples to the optical microscope and the goniometer/tensiometer, a brief air exposure was inevitable.

3. Kinetic modeling of run-in and steady-state COF

Friction originates from various forces resisting relative motion between two sliding bodies at the contacting interface under compressive

and shear stresses. The measured friction force, F_f [45,46], can be viewed as a sum of all contributions within the contact area of the two bodies [53–55]:

$$F_f = \mu \cdot F_N = \sum F_{local} \tag{1}$$

where F_N is the applied normal force, μ is the COF, and F_{local} is the friction force at a given local site within the contact area. F_{local} can vary depending on physical (surface roughness, local topography, mechanical property, etc.) and/or chemical (chemical functional group, reactivity, adsorbate, etc.) conditions [20,56–59]. Although these microscale or molecular scale factors may convolute the measured friction force in a sophisticated fashion [20], Eq. (1) can still be employed, as a first-order approximation, to determine changes in surface conditions during friction.

To use this approximation approach, one needs to know the μ of each representative surface condition. The RMS roughness of H-DLC is about 4 nm [39], which is smaller than the elastic deformation depth calculated from the Hertzian contact mechanics [39]. Thus, the surface roughness or topography effects would be negligible [45]. The local mechanical property dependence of μ could be lumped into a chemistry-dependent μ value. This is because *variations in local modulus and adhesion force due to chemical changes are coupled with the type and degree of surface oxidation* [60,61]; in other words, it is difficult to model the mechanical and chemical effects separately.

Then, the local chemical conditions of the H-DLC surface during friction test in reactive (oxidizing) environments can be assumed to be binary: unoxidized versus oxidized. The propensity of environmental oxidation is due to the presence of highly strained chemical bonds in the amorphous carbon deposited through the high-energy PECVD process [62,63]. The fact that H-DLC exhibits the run-in behavior [14,64] indicates that the oxidation states of the initial H-DLC surface formed in ambient air before the friction test [11,65] is different from those of the re-oxidized H-DLC surface during the friction test. To address all these observations, the chemical status of the H-DLC surface can be categorized into the following three: (i) the initial surface layer oxidized by humid air during the sample storage (before the friction test), (ii) the unoxidized (superlubricious) H-DLC surface exposed upon tribochemical wear of the oxidized surface layer, and (iii) the re-oxidized surface layer by reaction with O_2 or H_2O between consecutive sliding cycles (during the friction test).

Following Eq. (1), the COF measured at a given environmental condition, μ^{envr}, can be re-written as:

$$\mu^{envr}(n) = \mu_{ini}^{envr} \cdot \theta_{ini}^{envr}(n) + \mu_{HDLC} \cdot \theta_{HDLC}(n) + \mu_{RO}^{envr} \cdot \theta_{RO}^{envr}(n) \tag{2}$$

where n is the number of cycles of reciprocating friction test; μ_{ini}^{envr}, μ_{HDLC}, and μ_{RO}^{envr} are COF of the *initial* air-oxidized surface measured with the *pristine* counter-surface in the given environment, COF of the *unoxidized* H-DLC surface exposed by frictional shear and measured with the *unoxidized transfer film* at the counter-surface in inert condition [3,14], and COF of the *re-oxidized* surface measured with the *oxidized transfer film* in the given environment, respectively; and θ_{ini}^{envr}, θ_{HDLC}, and θ_{RO}^{envr} are fractional coverages of the corresponding surface conditions. Hereafter, the superscripts in these symbols will be replaced with actual environmental conditions such as N_2 for dry nitrogen, O_2 for dry oxygen (O_2 mixed with N_2), and H_2O for humid nitrogen (H_2O vapor in N_2). The sum of fractional coverages at any given cycle should be unity (entire sliding contact area). Here, μ_{HDLC} can be assumed to be the steady-state ultra-low COF of H-DLC after the run-in period measured in inert environment (i.e., after removal of all oxidized species by frictional wear) [30]. In humid condition, the surface represented by $\theta_{RO}^{H_2O}$ may be covered with physisorbed water molecule as well.

An important characteristics of the H-DLC oxidation in ambient air is that it stops at a self-limiting thickness [12,30,66]. For the sample that has been exposed to air, the thickness of the native oxide layer is measured to be ~ 2 nm [11,13]. It does not grow thicker, unless the sample is heated in air [31], likely due to the transport or diffusion limitation of oxidizing species in H-DLC [31]. This self-limiting behavior is similar to the Langmuir chemisorption model in which the surface coverage of the chemisorbed species grows to a maximum value limited by the reaction condition (≈ a monolayer in typical chemical reaction conditions) [33,34]. One can set this self-limiting thickness of the oxidized surface layer of H-DLC to be $\theta = 1$, regardless of the source of oxidizing environment. Then, θ_{RO}^{envr} is equivalent to the 'effective contribution' of the re-oxidized surface condition to the total friction measured experimentally within the contact area during the reciprocal sliding cycle.

Following the Langmuir kinetics model [33,34], the temporal change of surface coverage due to reactions in a given environmental condition, $\frac{d\theta}{dt}$, can be expressed as:

$$\frac{d\theta}{dt} = k_{RO} \cdot (1 - \theta) - k_{des} \cdot \theta \tag{3}$$

where k_{RO} and k_{des} are the oxidation rate constant of H-DLC by a specific source gas and the thermal desorption rate constant of the reaction product, respectively. In Eq. (3), super- and sub-scripts of k and θ are omitted for simplicity. The k_{RO} term can be expressed as the reaction probability per collision, a_{RO}^{envr}, times the collision frequency of the reactive gas molecule at a given pressure, P_{gas}. Here, k_{des} can be set to zero at room temperature because the oxidized surface layer is stable and remains intact even in ultra-high vacuum conditions [8,67]. In principle, a_{RO}^{envr} term can change with temperature; but in practice, it can be assumed to be constant because the local temperature rise caused by frictional heat during sliding on H-DLC surface is negligible unless the sliding speed is extremely high (see Supporting Information). By integrating Eq. (3) with respect to time, the following time-dependent fractional coverage equation can be obtained:

$$\theta(t) = 1 - (1 - \theta(t_0)) \cdot \exp(-k_{RO} \cdot (t - t_0)) \tag{4}$$

where t_0 is the time at which the surface is emerged out of the sliding contact and t is the time exposed to the given environment after the contact.

In the reciprocating friction test, mechanical or tribochemical removals of the oxidized surface species take place during the sliding contact, and oxidized species are re-formed between the consecutive sliding contacts. Hence, $\theta(t)$ becomes a cycle-dependent variable during tribo-test in the reactive environmental condition. Thus, Eq. (4) is further converted into a recursive form:

$$\theta(n) = 1 - (1 - (1 - \gamma_{removal}) \cdot \theta(n-1)) \cdot \exp(-k_{RO} \cdot t_{cycle}) \tag{5}$$

where $\theta(n)$ is the fractional coverage at n^{th} friction cycle, $\theta(n-1)$ means the fractional coverage after the previous sliding cycle which replaces $\theta(t_0)$ in Eq. (4), t_{cycle} is the interval between two consecutive sliding cycles which replaces $(t - t_0)$ in Eq. (4), and $\gamma_{removal}$ is the removal probability of the oxidized surface species during each sliding contact ($0 \le \gamma_{removal} \le 1$). The details of the derivation of $\theta(n)$ as a function of $\gamma_{removal}$ can be found elsewhere [24,25,68,69]. The $\gamma_{removal}$ will depend on not only physical conditions such as contact stress, sliding speed, and surface roughness (which may vary due to wear) [24,25,69], but also chemical conditions (chemical species of oxidized H-DLC or transfer film at given environmental conditions). At a given mechanical sliding condition, $\gamma_{removal}$ can be modeled as a single value for simplification. Even if there are multiple parameters or processes affecting $\gamma_{removal}$, their individual contributions cannot be determined in COF measurements anyhow.

It is difficult to study individual effects of O_2 and H_2O in humid air; thus, those effects are studied separately in dry O_2 ($O_2 + N_2$ mixture) or humid N_2 ($H_2O + N_2$ mixture) at ambient pressure. The details of COF fitting process to derive $\gamma_{removal}$ and a_{RO} at a given environment can be

found in the Supporting Information.

The fit result is physically meaningful only within the validity limit of the assumptions made in this kinetics modeling. Borrowing the Langmuir reaction kinetics, the local oxidation state is assumed to be binary – unoxidized or oxidized. In our model, the local oxidation states of the H-DLC surface are further distinguished into two: 'oxidized by ambient air during the sample storage' versus 'oxidized by reactive gas during the friction test'. A similar model can also be applied to other systems that have initial native oxide layers and show a transient period before reaching a steady-state friction; examples include copper-impregnated metallized carbon surface [70] and Co-Cr-Mo alloy surface [71].

One could add additional parameters such as partial or gradual removal of the oxidized layer or diffusion of reactive species into the subsurface to reach the self-limiting thickness. However, these additional parameters just increase the degree of freedom in the model, causing instability in mathematical fitting of experimental data collected with limited independent variables. Thus, such details cannot be modeled using the Langmuir reaction kinetics. We also set μ_{ini}^{envr} as the COF of the *initial* air-oxidized surface measured with the *pristine* counter-surface. In reality, it will gradually change from the COF measured with the pristine counter-surface to the COF measured with the transfer film formed at the counter-surface. Practically, it is difficult to measure the cycle dependence of the transfer film coverage on the counter-surface without affecting the surface condition of the H-DLC substrate. So, to keep the degree of freedom minimum in the fitting algorithm, we use one constant value for μ_{ini}^{envr}.

4. Results and discussion

4.1. Determination of μ_{ini}^{envr}, μ_{HDLC}, and μ_{RO}^{envr}

To use the kinetics model described in Section 3, the magnitude of μ_{ini}^{envr}, μ_{RO}^{envr}, and μ_{HDLC} must be determined first because the local oxidation states of H-DLC were assumed to be binary in the model – oxidized or unoxidized. Therefore, it needs to measure COFs of (i) the *initial* air-oxidized H-DLC measured with the *pristine* counter body at a given environment, (ii) the fully *re-oxidized* H-DLC measured with the *oxidized transfer film* at a given environment, and (iii) the *un-oxidized* H-DLC produced by frictional wear and measured with the *un-oxidized transfer film* in inert condition. Fig. 1 plots those COFs measured in each environmental condition. At the beginning of the run-in process in dry N_2, the COF of the initial air-oxidized surface [11,72] is 0.263 ± 0.007 (left panels in Fig. 1), which can be taken as $\mu_{ini}^{N_2}$. The $\mu_{ini}^{O_2}$ and $\mu_{ini}^{H_2O}$ are very similar to this value (see Fig. 2a and 3a). As the initial air-oxidized layer wears off due to frictional shear and the transfer film is formed on the counter surface during the run-in process, the COF decreases to 0.012 ± 0.001which can be considered as μ_{HDLC} [3,15,73]. When friction of the initial air-oxidized surface is measured with the fully-developed transfer film on the counter surface, the COF value is somewhat lower (0.142 ± 0.025; see top panel in Fig. 1) than $\mu_{ini}^{N_2}$. But the exact transition between these two conditions is difficult to find; so, $\mu_{ini}^{N_2}$ is used in the fitting with the kinetics model.

To determine $\mu_{RO}^{O_2}$ and $\mu_{RO}^{H_2O}$, the H-DLC surface was first rubbed with the SS ball in dry N_2 until μ_{HDLC} was achieved to produce *unoxidized* transfer film, and then exposed to dry O_2 (P_{O_2} = 228 Torr in N_2) or humid N_2 (P_{O_2} = 7.1 Torr, which corresponds to 30% RH), respectively, with the counter-surface disengaged for 5 min, and finally re-engaged with the same (but now oxidized) transfer film for friction measurement at the same sliding track without altering the environment condition. This control test shows $\mu_{RO}^{O_2} = 0.076 \pm 0.014$ (middle panel in Fig. 1) and$\mu_{RO}^{H_2O} = 0.200 \pm 0.005$ (bottom panel in Fig. 1). The $\mu_{RO}^{H_2O}$ value is quite comparable with the COF observed for the single-layer thick graphene step edge terminated with OH groups [18]. This implies that the magnitude of COF is mostly governed by chemical interactions between the substrate and the counter-surface for the carbon surfaces.

4.2. Analysis of $\mu^{O_2}(n)$ and $\mu^{H_2O}(n)$ of H-DLC with Langmuir-type kinetics model

Fig. 2a and 3a display the $\mu^{O_2}(n)$ and $\mu^{H_2O}(n)$ of H-DLC measured in various P_{O_2} and P_{H_2O} conditions, respectively. In each condition, triplicate measurements confirmed the reproducibility of the data. To avoid fitting uncontrollable noises, the averaged data were used for the analysis with the kinetics model derived in Section 3. First, the steady-state portions of the data, for example, $\mu^{O_2}(ss; P_{O_2})$, were fitted using Eq. (5) and Eq. (7) of the Supporting Information to obtain $a_{RO}^{O_2}$ and $\gamma_{RO}^{O_2}(P_{O_2})$. Similarly, the $\mu^{H_2O}(ss; P_{H_2O})$ data were fitted with Eq. (5) and Eq. (9) of the Supporting Information to get $a_{RO}^{H_2O}$ and $\gamma_{RO}^{H_2O}(P_{H_2O})$. The re-oxidation probability was set to be constant and independent of partial pressure in

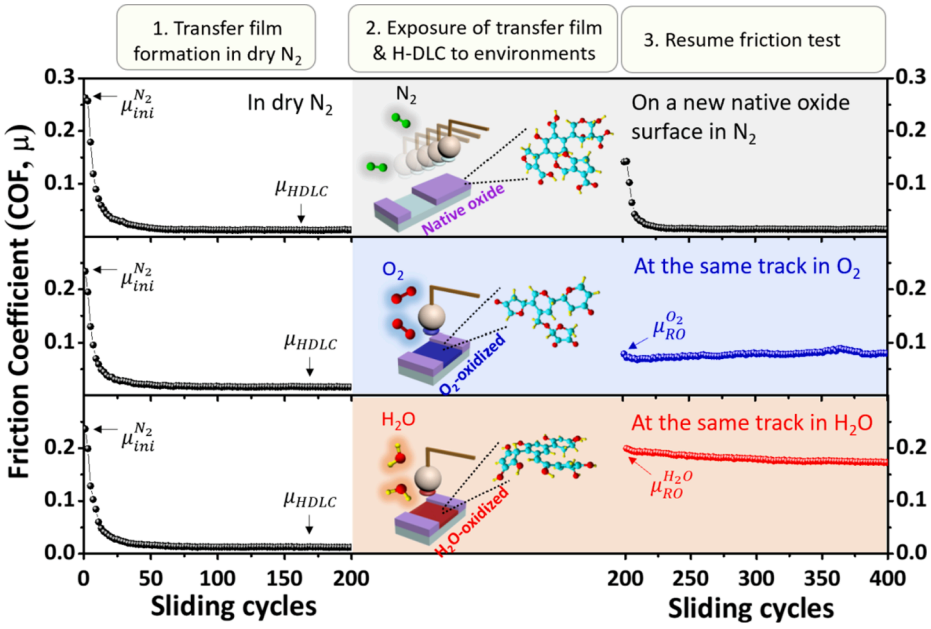

Fig. 1. COF of H-DLC as a function of reciprocating cycle in different environmental conditions. Initially, the H-DLC film coated with the air-oxidized layer was tribo-tested in dry N_2. After 200 cycles of reciprocating sliding, the counter-surface was lifted and the wear track of the substrate and the transfer film on the counter-surface were exposed to dry N_2 (O_2 < 4 ppm, H_2O < 3 ppm), N_2 mixed with O_2 (P_{O_2} = 228 Torr), and humid N_2 (P_{H_2O} = 7.1 Torr) for 5 min. Then, the counter-surface was re-engaged with the substrate and measured friction at a different location in dry N_2 and at the same wear track in O_2 and H_2O environments.

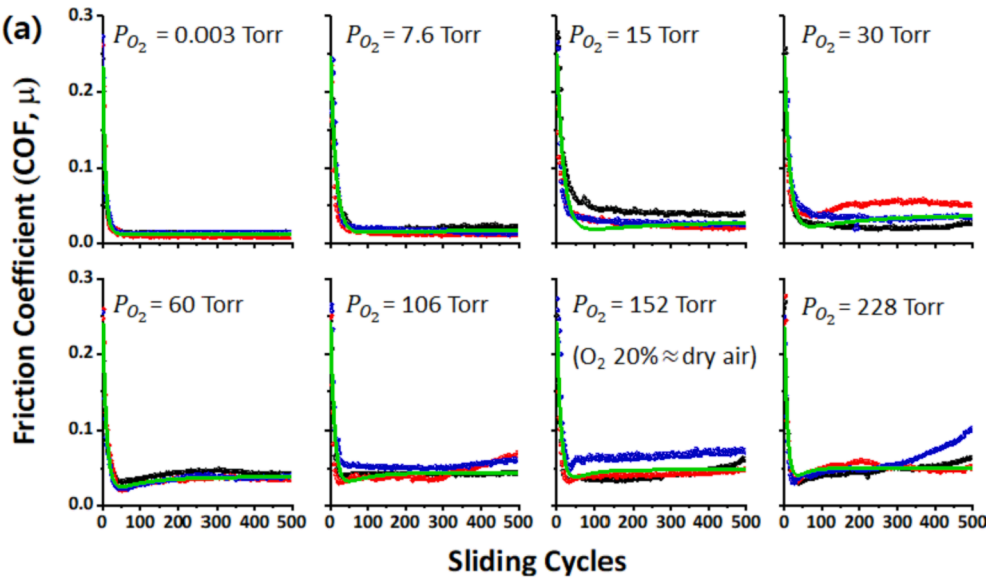

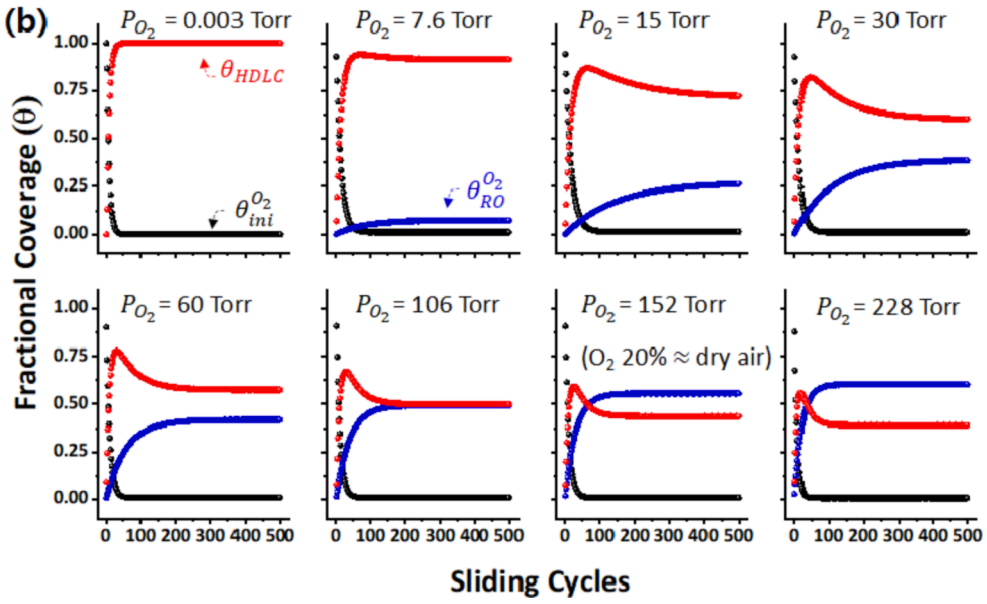

Fig. 2. (a) COF change as a function of reciprocating cycle, $\mu^{O_2}(n)$, in various P_{O_2} conditions in N_2. Three measurements data are shown with black, red, and blue symbols; the green symbols are the numerical fit result with the values of $\mu_{ini}^{O_2} = 0.263 \pm 0.007$, $\mu_{RO}^{O_2} = 0.076 \pm 0.014$, $\mu_{HDLC} = 0.012 \pm 0.001$, and $t_{cycle} = 1.61s$. (b) Fraction coverages calculated from the fit: black = $\theta_{ini}^{O_2}$; red = θ_{HDLC}; blue = $\theta_{RO}^{O_2}$. (For interpretation of the references to colour in this figure legend, the reader is referred to the web version of this article.)

the given reactive condition because it is a function of temperature and reactive species [note that the re-oxidation rate is a function of partial pressure]. The removal probability was allowed to vary depending on the partial pressure during data fitting; this was especially necessary to account for the boundary lubrication effect of the adsorbed molecular water (more details are described later). Next, the entire $\mu^{O_2}(n)$ and $\mu^{H_2O}(n)$ data – both run-in and steady-state regions – were fitted with Eqs. (6) and (10) shown in the Supporting Information, respectively. The fit results are shown as green lines in Fig. 2a and 3a. The changes in fractional coverages, $\theta_{ini}^{envr}(n)$, $\theta_{HDLC}(n)$, and $\theta_{RO}^{envr}(n)$, are plotted in Fig. 2b and 3b for each partial pressure condition.

The run-in period can be defined as the number of reciprocating cycles at which the $\mu^{envr}(n)$ value decreases by 90% of the difference between the initial and steady-state values, $0.9 \times (\mu^{envr}(1) - \mu^{envr}(ss))$. In dry N_2 environment, the run-in period is typically 15 ~ 16 cycles, implying that most of the initial air-oxidized layer wears off easily and the unoxidized superlubricious H-DLC surface is exposed in the wear track. The molecular origin for the superlubricity of H-DLC surfaces is still in debate. The superlubricity may not come from a single origin, and multiple factors may have to work together. Those include the absence of oxidizing gases in the environment, sufficient passivation of carbon surfaces with hydrogen, and sp^2-rich graphitic transformation of the shear plane [2–5,15,39,74,75]. The atomic smoothness (as in the case of graphene or graphite basal plane) is not necessary; based on the graphene step-edge study, it appears that as long as the topographic corrugation is small enough and the surface is inert, the measured COF would be ultra-low [76]. In the absence of oxidizing gas molecules in the environment (as in vacuum) [77–79] or when their concentration is sufficiently low enough (as in the case of dry nitrogen) [3–5], the surface condition in the sliding track of H-DLC is readily converted to and kept in the superlubricious state.

As P_{O_2} increases, the run-in duration increases to 30 ~ 40 cycles in the 7.6 ~ 30 Torr regime and then decreases back to ~ 15 cycles in the high O_2 concentration regime (Fig. 2a). It is interesting to see that $\mu^{O_2}(n)$ decreases slightly below the $\mu^{O_2}(ss)$ value and then gradually approaches to the $\mu^{O_2}(ss)$ value. The kinetics modeling results show that θ_{HDLC} negatively correlates with the decrease of $\theta_{ini}^{O_2}$ until it reaches a

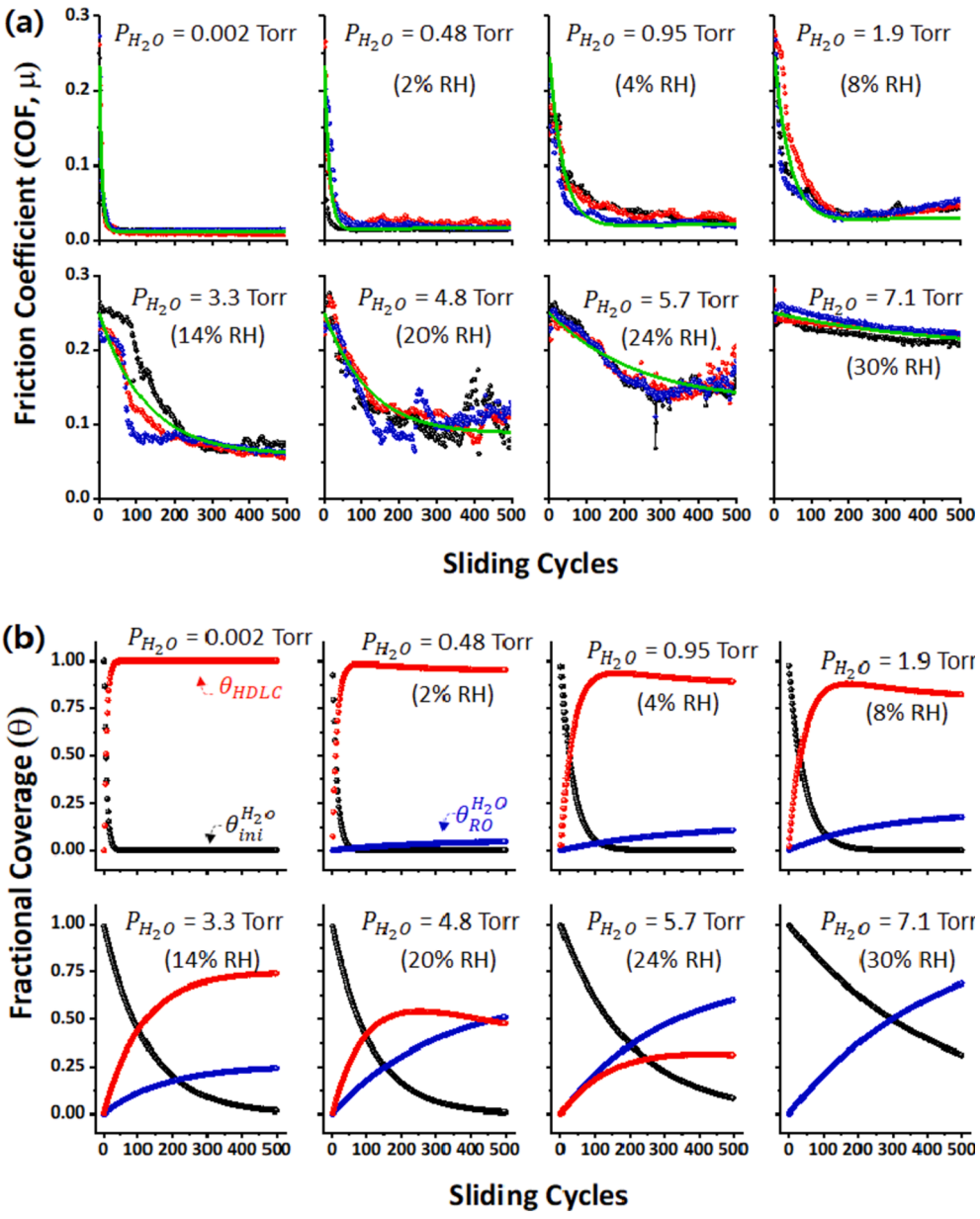

Fig. 3. (a) COF change as a function of reciprocating cycle, $\mu^{H_2O}(n)$, in various P_{H_2O} conditions in N_2. Three measurements data are shown with black, red, and blue symbols; the green symbols are the numerical fit result with the values of $\mu_{ini}^{H_2O} \approx 0.251 \pm 0.025$, $\mu_{RO}^{H_2O} = 0.200 \pm 0.005$, $\mu_{HDLC} = 0.012 \pm 0.001$, and $t_{cycle} = 1.61s$. (b) Fraction coverages calculated from the fit: black = $\theta_{ini}^{H_2O}$; red = θ_{HDLC}; blue = $\theta_{RO}^{H_2O}$. (For interpretation of the references to colour in this figure legend, the reader is referred to the web version of this article.)

maximum value and then gradually decreases to the steady-state value which varies depending on P_{O_2} (Fig. 2b). The decreasing and leveling-off portions of θ_{HDLC} negatively correlate with $\theta_{RO}^{O_2}$. This trend indicates that the two competing processes – (i) removal of the initially-oxidized layer exposing superlubricious H-DLC surface and (ii) re-oxidation of the newly-exposed H-DLC surface – are taking place at different rates.

It is also interesting to note that the $\mu^{O_2}(ss)$ is relatively low, around 0.05 even at$P_{O_2} = 152$ Torr which corresponds to dry air (Fig. 2a). This is because the COF of O_2-oxidized surface is low ($\mu_{RO}^{O_2} = 0.076 \pm 0.014$) and the re-oxidized surface fraction is kept at around 0.5 at the steady state (Fig. 2b). In other words, the surface species formed by re-oxidation of H-DLC in O_2 is readily removed by friction. More details will be discussed in Section 4.3.

In humid N_2 environment, there is a noticeable increase in both $\mu^{H_2O}(ss)$ and run-in duration, as compared to dry N_2 and dry O_2 conditions. As P_{H_2O} increases, $\mu^{H_2O}(ss)$ approaches a value typical for boundary lubrication by physisorbed molecular species present at the shear plane (around 0.15–0.20) [80–82]. The lengthening of the run-in period could mean less wear of the initial air-oxidized layer per cycle (or its survival for an extended period), which is consistent with the notion that a 'protective' boundary lubrication layer is formed as P_{H_2O} increases. The physisorbed molecular water species can act as a boundary lubrication layer and, in the absence of any mechanical shear of the surface, the monolayer of adsorbed water can be formed on the air-oxidized H-DLC surface at RH around 20% [83].

It is expected that the H_2O-oxidized H-DLC surface will contain hydroxyl (OH) groups that can facilitate water adsorption from humid environments. Unfortunately, the air exposure during the sample transfer to the XPS system after tribo-test in controlled environments complicates the quantification of surface functional groups at the O_2 and H_2O exposed H-DLC surfaces [12]. Even though not quantitative, water condensation and wetting behaviors can still be used to differentiate the chemistry of the H-DLC surface oxidized during the tribo-test in different environmental conditions. On a hydrophilic surface, the water condensation droplet density is higher, and the droplet size is smaller, as compared to a hydrophobic surface [84,85]. Fig. 4a-c displays optical images of water droplets formed by condensation at the saturation RH condition on H-DLC surfaces tribo-tested in different environmental

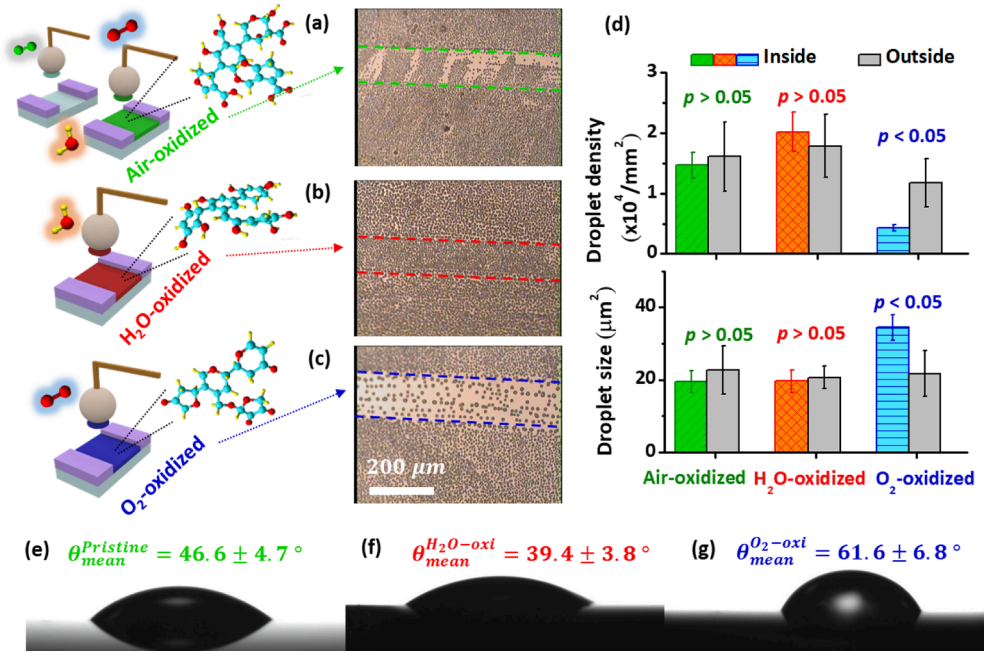

Fig. 4. (a-c) Optical microscope images showing differences in water condensation behaviors on H-DLC surface tribo-tested in (a) dry nitrogen, (b) humid nitrogen (P_{H_2O} = 7.1 Torr), and (c) dry O_2 (P_{O_2} = 228 Torr). The wear track in (a) was oxidized upon exposure to air during the sample transfer. The wear tracks in (b) and (c) were oxidized by H_2O and O_2 exposure during the tribo-test; but it was likely to be oxidized further during the sample transfer [12]. (d) Condensed water droplet density and size. The statistics were obtained from three replicates of water condensation tests. The p-value of the student's *t*-test is also shown for the comparison between the inside and outside regions of the wear track. (e-g) Water contact angle on (e) air-oxidized surface after friction test in dry nitrogen, (f) H_2O-oxidized surface during friction test in humid nitrogen, and (g) O_2-oxidized surface during friction test in dry O_2.

conditions. In the wear track produced in the dry N_2 tribo-test and then oxidized upon subsequent exposure to humid lab air, the water condensation shows patchy behaviors – a mix of highly-dense and sparsely-distributed areas. In the wear tracks produced in humid N_2 and dry O_2, the water condensation appears to be more homogeneous. Fig. 4d plots the density and size of droplets formed by water condensation. Although statistically insignificant, the H_2O-oxidizd wear track appears slightly more hydrophilic than the outside region which can be considered as a reference for comparison. In contrast, the O_2-oxidized surface is significantly more hydrophobic than the H_2O– and air-oxidized surfaces. The water contact angle data shown in Fig. 4e-g are consistent with the water condensation data. In the Wenzel model [86], the contact angle depends on the surface roughness factor or the ratio of actual surface area to projected surface area. However, the surface roughness effect of H-DLC films induced by frictional wear is negligible since the wear depth (~25 nm at maximum in Fig. 6b) is around three orders smaller than the Hertzian contact diameter (~60 μm). Therefore, the effect of the surface roughness change due to wear on the water contact angle can be ignored. These results support the hypothesis that water adsorption occurs readily on the H_2O-oxidized wear track, which will act as the boundary lubrication layer.

4.3. Comparison of tribochemical kinetics of H-DLC in O_2 and H_2O environments

The physical parameters determined from the Langmuir-type kinetics analysis of the $\mu^{O_2}(n)$ and $\mu^{H_2O}(n)$ data are plotted in Fig. 5. The oxidation reaction probability, calculated from the rate constant plot in Fig. 5a, is on the order of 10^{-5}–10^{-4} Torr^{-1} s^{-1}. Since the collision frequency of a gas molecule at the surface is ~ 7×10^9 s^{-1} at 760 Torr at room temperature (calculated for N_2; the values for O_2 and H_2O are in the same order of magnitude) [87], the absolute reaction probability per collision is quite low. Nonetheless, this value is only one or two orders of magnitude lower than typical reaction probability of reactive gases on catalytically-active surfaces (for example, ~10^{-3} Torr^{-1} s^{-1} for hydrogenation of cyclohexene on Pt, Pd, and Rh) [88–90]. This high reactivity must be due to the intrinsic nature of amorphous carbon surface produced by high-energy PECVD process which inevitably has broad distributions of C-C bond lengths and C-C-C angles that deviate from those of thermodynamically-stable diamond or graphite [62,63].

The re-oxidation probability of the freshly-exposed H-DLC surface is ~ 5 times higher for H_2O than O_2. The higher reaction probability with H_2O is probably due to a high sticking probability of H_2O during the

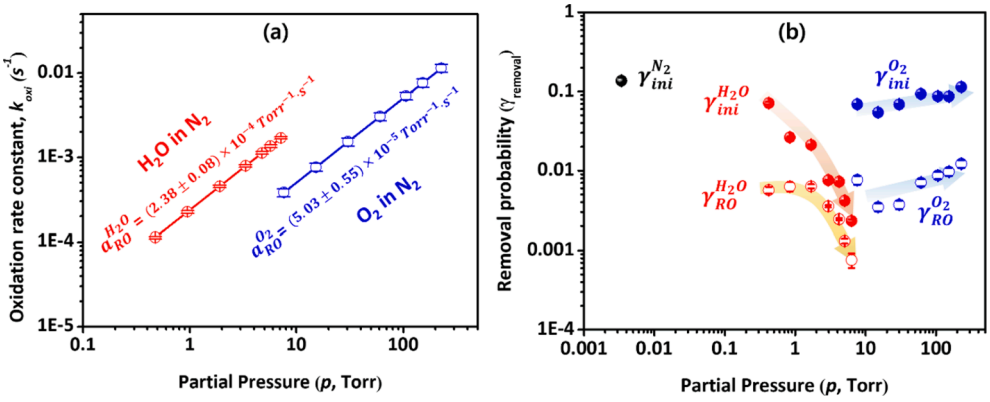

Fig. 5. (a) Oxidation rate constant of the newly-exposed H-DLC surface and (b) removal probability of the initial air-oxidized surface during the sample storage and the re-oxidized surface during the friction test. In (a), the slope corresponds to the reaction probability of the H-DLC surface per Torr per sec. In (b), the filled and open symbols are the removal probabilities of the initial air-oxidized and re-oxidized surfaces, respective, in the environmental condition denoted in the superscript.

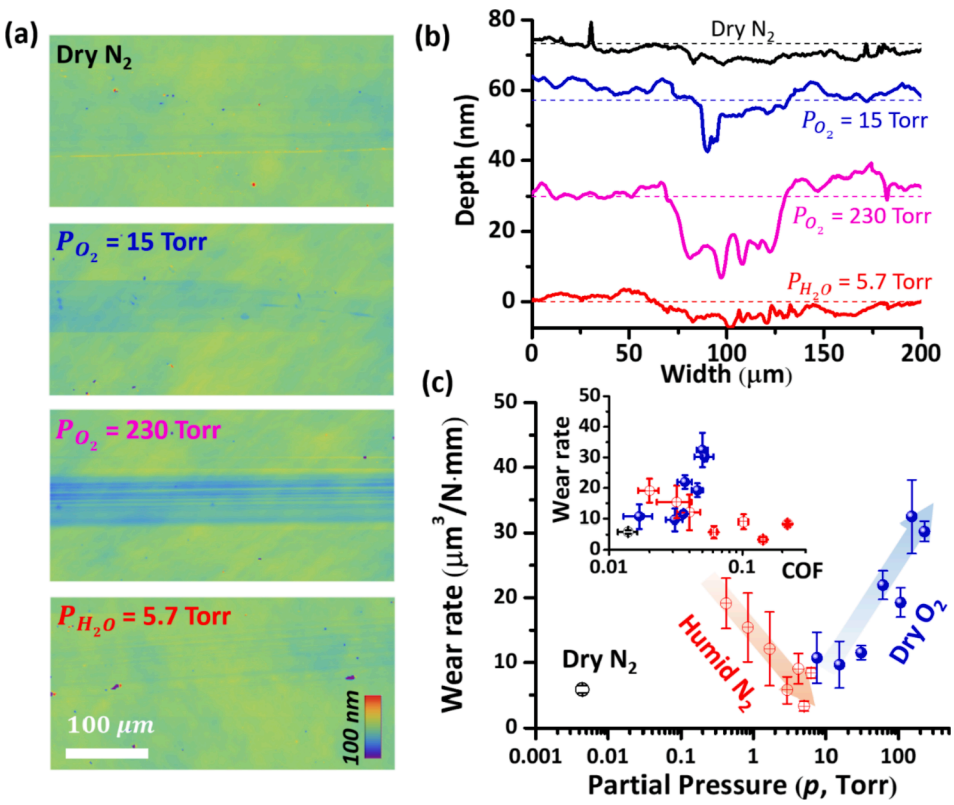

Fig. 6. (a) Optical profilometry images and (b) line profiles of representative wear tracks produced after 500 reciprocating cycles in different environmental conditions. (c) Plot of wear rate versus partial pressure of H_2O and O_2 in nitrogen at ambient pressure. The wear rate was calculated with the total wear volume after 500 cycles. The inset plots to wear rate versus COF measured in different environmental conditions. Wear track images of other conditions are shown in the Supporting Information.

physisorption process, which increases the residence time of H_2O molecules at the surface. Such a physisorption process does not occur for O_2 on oxide surfaces at room temperature [81,91]. In this study, the true reaction probability cannot be obtained since the friction measurement cannot distinguish contributions from the physisorbed (intact) or chemisorbed (reacted) states of H_2O on the surface.

The removal probability per sliding cycle is shown for the initial air-oxidized layer and the re-oxidized species is shown in Fig. 5b. In dry N_2, $\gamma_{ini}^{N_2}$ is quite high, around 0.1, reflecting the very short run-in period before μ^{N_2} reaches the μ_{HDLC} value. In the humid condition, $\gamma_{ini}^{H_2O}$ gradually decreases from the $\gamma_{ini}^{N_2}$ value to $\sim 0.0023 \pm 0.0001$ as P_{H_2O} increases from ~ 0.002 Torr to 7.1 Torr. As discussed in Section 4.2, this can be attributed to the boundary lubrication effect as the coverage of the physisorbed molecular water layer increases [39,82]. The $\gamma_{RO}^{H_2O}$ of the H_2O-oxidized species is about one order of magnitude lower than $\gamma_{ini}^{H_2O}$ at$P_{H_2O} = 0.48$ Torr and decreases further by another order of magnitude as P_{H_2O} increases to 7.1 Torr (=30% RH) at which the formation of full monolayer of adsorbed waters is expected [83].

Since there is no boundary lubrication effect of physisorbed molecules in the dry O_2 environment, $\gamma_{ini}^{O_2}$ remains almost unchanged from $\gamma_{ini}^{N_2}$. For the re-oxidized surface species in dry O_2, $\gamma_{RO}^{O_2}$ is about one order of magnitude lower than $\gamma_{ini}^{O_2}$, implying that the re-oxidized species during the tribo-test is not as readily removable as the initial air-oxidized layer. This must be due to the difference in surface chemistry between these surfaces oxidized under different conditions (see Fig. 4). Its P_{O_2} dependence is found to be relatively weak, which is again due to the absence of any physisorbed molecules at the surface. Because the oxidation rate increases linearly with P_{O_2} (Fig. 5a), the relatively constant $\gamma_{RO}^{O_2}$ means that the effective wear rate will increase with P_{O_2}.

To confirm this prediction, the wear rates of H-DLC during the tribo-test in dry N_2, humid N_2, and dry O_2 environments were measured using optical profilometry and the results are shown in Fig. 6. In dry N_2, the wear rate of H-DLC is extremely low once the run-in period ceases because the surface is in the superlubricious state [3,15,30]. In dry O_2 environments, the wear rate increases monotonically (Fig. 6c). Our kinetics analysis indicates that this is simply because the oxidation rate increases linearly with P_{O_2} (Fig. 5a), while the removal probability of the re-oxidized species remains fairly constant (Fig. 5b). In contrast, the wear rate decreases as P_{H_2O} increases (Fig. 6a) although the re-oxidation rate increases with P_{H_2O} (Fig. 5a). Once again, this can be ascribed to the boundary lubrication effect of physisorbed water layers.

The inset of Fig. 6c plots the experimental wear rate versus the measured COF. This plot clearly shows that the absolute COF value is not a good descriptor that can be used to predict the wear rate of H-DLC. In the case of humid environments, the wear rate decreases even though COF increases. This is because the COF of boundary lubrication by physisorbed molecules are higher than μ_{HDLC}.

5. Conclusions

The tribochemical effects of oxygen gas (O_2) and water vapor (H_2O) on friction and wear of H-DLC were elucidated by analyzing the reciprocating cycle dependence of friction coefficient with the Langmuir-type kinetics model. The H-DLC surface exposed by frictional wear is readily oxidized by O_2 and H_2O impinging from the gas phase. The re-oxidation probability of the H-DLC surface exposed by frictional wear is found to be only one or two magnitudes lower than the reaction probability of highly-reactive catalysts. The O_2-oxidixed surface retains low friction but is vulnerable to shear-driven wear. The H_2O-oxidized surface becomes resistant to wear due to the boundary lubrication effect of adsorbed water molecules in humid conditions, but its friction is relatively high due to the adsorbed water layer. These findings provide deeper insights into tribochemical oxidation processes of engineering device systems coated with H-DLC films in ambient conditions. The kinetic model derived in this study can also be employed to describe environmental effects on lubrication performances of other solid lubricant films.

CRediT authorship contribution statement

Seokhoon Jang: Investigation, Data curation, Methodology, Validation, Formal analysis, Writing – original draft, Writing – review & editing. **Zhe Chen:** Investigation, Writing – review & editing. **Seong H. Kim:** Conceptualization, Investigation, Data curation, Methodology, Validation, Formal analysis, Writing – review & editing, Supervision, Project administration, Funding acquisition.

Declaration of Competing Interest

The authors declare that they have no known competing financial interests or personal relationships that could have appeared to influence the work reported in this paper.

Acknowledgements

This work was supported by the National Science Foundation (Grant No. CMMI-1912199). The authors acknowledge Prof. Ali Erdemir for providing H-DLC samples for this study and Prof. Ashlie Martini and Prof. Brian Borovsky for discussions.

Appendix A. Supplementary data

Supplementary data to this article can be found online at https://doi.org/10.1016/j.apsusc.2021.152299.

References

[1] A. Erdemir, O.L. Eryilmaz, I.B. Nilufer, G.R. Fenske, Synthesis of superlow-friction carbon films from highly hydrogenated methane plasmas, Surf. Coat. Technol. 133-134 (2000) 448–454.
[2] A. Erdemir, C. Donnet, Tribology of diamond-like carbon films: recent progress and future prospects, J. Phys. D Appl. Phys. 39 (18) (2006) R311–R327.
[3] P. Manimunda, A. Al-Azizi, S.H. Kim, R.R. Chromik, Shear-Induced Structural Changes and Origin of Ultralow Friction of Hydrogenated Diamond-like Carbon (DLC) in Dry Environment, ACS Appl. Mater. Interfaces 9 (19) (2017) 16704–16714.
[4] J.C. Sánchez-López, A. Erdemir, C. Donnet, T.C. Rojas, Friction-induced structural transformations of diamondlike carbon coatings under various atmospheres, Surf. Coat. Technol. 163-164 (2003) 444–450.
[5] H.I. Kim, J.R. Lince, O.L. Eryilmaz, A. Erdemir, Environmental effects on the friction of hydrogenated DLC films, Tribol. Lett. 21 (1) (2006) 51–56.
[6] H. Li, T. Xu, C. Wang, J. Chen, H. Zhou, H. Liu, Humidity dependence on the friction and wear behavior of diamond-like carbon film in air and nitrogen environments, Diam. Relat. Mater. 15 (2006) 1585–1592.
[7] H. Li, T. Xu, C. Wang, J. Chen, H. Zhou, H. Liu, Tribochemical effects on the friction and wear behaviors of a-C: H and a-C films in different environment, Tribol. Int. 40 (2007) 132–138.
[8] O.L. Eryilmaz, A. Erdemir, Surface analytical investigation of nearly-frictionless carbon films after tests in dry and humid nitrogen, Surf. Coat. Technol. 201 (2007) 7401–7407.
[9] O.L. Eryilmaz, A. Erdemir, Investigation of initial and steady-state sliding behavior of a nearly frictionless carbon film by imaging 2-and 3-D TOF-SIMS, Tribol. Lett. 28 (2007) 241–249.
[10] H. Li, T. Xu, C. Wang, J. Chen, H. Zhou, H. Liu, Friction-induced physical and chemical interactions among diamond-like carbon film, steel ball and water and/or oxygen molecules, Diam. Relat. Mater. 15 (2006) 1228–1234.
[11] M. Yang, M.J. Marino, V.J. Bojan, O.L. Eryilmaz, A. Erdemir, S.H. Kim, Quantification of oxygenated species on a diamond-like carbon (DLC) surface, Appl. Surf. Sci. 257 (2011) 7633–7638.
[12] M.J. Marino, E. Hsiao, Y. Chen, O.L. Eryilmaz, A. Erdemir, S.H. Kim, Understanding run-in behavior of diamond-like carbon friction and preventing diamond-like carbon wear in humid air, Langmuir 27 (2011) 12702–12708.
[13] N.J. Mehta, S. Roy, J.A. Johnson, J. Woodford, A. Zinovev, Z. Islam, A. Erdemir, S. Sinha, G. Fenske, B. Prorok, X-ray studies of near-frictionless carbon films, MRS Online Proceedings Library 843 (2004) 271–276.
[14] T. Scharf, I. Singer, Monitoring transfer films and friction instabilities with in situ Raman tribometry, Tribol. Lett. 14 (2003) 3–8.
[15] T.W. Scharf, I.L. Singer, Role of the Transfer Film on the Friction and Wear of Metal Carbide Reinforced Amorphous Carbon Coatings During Run-in, Tribol. Lett. 36 (2009) 43–53.
[16] A.P. Merkle, A. Erdemir, O.L. Eryilmaz, J.A. Johnson, L.D. Marks, In situ TEM studies of tribo-induced bonding modifications in near-frictionless carbon films, Carbon 48 (2010) 587–591.
[17] Z.-l. Wang, Elastic and inelastic scattering in electron diffraction and imaging, Springer Science & Business Media, 2013.
[18] Z. Chen, A. Khajeh, A. Martini, S.H. Kim, Identifying Physical and Chemical Contributions to Friction: A Comparative Study of Chemically Inert and Active Graphene Step Edges, ACS Appl. Mater. Interfaces 12 (2020) 30007–30015.
[19] Z. Chen, A. Khajeh, A. Martini, S.H. Kim, Origin of High Friction at Graphene Step Edges on Graphite, ACS Appl. Mater. Interfaces 13 (2021) 1895–1902.
[20] Z. Chen, A. Khajeh, A. Martini, S.H. Kim, Chemical and physical origins of friction on surfaces with atomic steps, Sci. Adv. 5 (8) (2019), https://doi.org/10.1126/sciadv.aaw0513.
[21] Y. Wang, J. Xu, Y. Ootani, S. Bai, Y. Higuchi, N. Ozawa, K. Adachi, J.M. Martin, M. Kubo, Tight-Binding Quantum Chemical Molecular Dynamics Study on the Friction and Wear Processes of Diamond-Like Carbon Coatings: Effect of Tensile Stress, ACS Appl. Mater. Interfaces 9 (39) (2017) 34396–34404.
[22] L. Dai, V. Sorkin, Y.-W. Zhang, Effect of Surface Chemistry on the Mechanisms and Governing Laws of Friction and Wear, ACS Appl. Mater. Interfaces 8 (13) (2016) 8765–8772.
[23] J.A. Heimberg, K.J. Wahl, I.L. Singer, A. Erdemir, Superlow friction behavior of diamond-like carbon coatings: Time and speed effects, Appl. Phys. Lett. 78 (17) (2001) 2449–2451.
[24] F.M. Borodich, L.M. Keer, Modeling effects of gas adsorption and removal on friction during sliding along diamond-like carbon films, Thin Solid Films 476 (1) (2005) 108–117.
[25] F.M. Borodich, C.S. Korach, L.M. Keer, Modeling the Tribochemical Aspects of Friction and Gradual Wear of Diamond-Like Carbon Films, J. Appl. Mech. 74 (1) (2007) 23, https://doi.org/10.1115/1.2172267.
[26] S.Y. Elovich, O. Larinov, Theory of adsorption from solutions of non electrolytes on solid (I) equation adsorption from solutions and the analysis of its simplest form, (II) verification of the equation of adsorption isotherm from solutions, Izv. Akad. Nauk. SSSR, Otd. Khim. Nauk 2 (1962) 209–216.
[27] J. Wang, X. Guo, Adsorption kinetic models: Physical meanings, applications, and solving methods, J Hazard Mater 390 (2020) 122156, https://doi.org/10.1016/j.jhazmat.2020.122156.
[28] J. Wang, L. Shang, X. Li, Z. Lu, G. Zhang, Quantifying macroscopic friction of diamond-like carbon films by microscopic adsorption and removal of water molecules, Langmuir 34 (1) (2018) 58–65.
[29] P.L. Dickrell, N. Argibay, O.L. Eryilmaz, A. Erdemir, W.G. Sawyer, Temperature and Water Vapor Pressure Effects on the Friction Coefficient of Hydrogenated Diamondlike Carbon Films, J. Tribol. 131 (2009).
[30] A.A. Al-Azizi, O. Eryilmaz, A. Erdemir, S.H. Kim, Surface structure of hydrogenated diamond-like carbon: origin of run-in behavior prior to superlubricious interfacial shear, Langmuir 31 (5) (2015) 1711–1721.
[31] C.T. Campbell, Transition metal oxides: extra thermodynamic stability as thin films, Phys Rev Lett 96 (2006) 066106.
[32] S. Azizian, S. Eris, L.D. Wilson, Re-evaluation of the century-old Langmuir isotherm for modeling adsorption phenomena in solution, Chem. Phys. 513 (2018) 99–104.
[33] I. Langmuir, The Constitution and Fundamental Properties of Solids and Liquids. Part I. Solids, J. Am. Chem. Soc. 38 (1916) 2221–2295.
[34] I. Langmuir, The adsorption of gases on plane surfaces of glass, mica and platinum, J. Am. Chem. Soc. 40 (1918) 1361–1403.
[35] A. Grill, B.S. Meyerson, V.V. Patel, J.A. Reimer, M.A. Petrich, Inhomogeneous carbon bonding in hydrogenated amorphous carbon films, J. Appl. Phys. 61 (1987) 2874–2877.
[36] A. Grill, V. Patel, Characterization of diamondlike carbon by infrared spectroscopy? Appl. Phys. Lett. 60 (1992) 2089–2091.
[37] M. Weiler, S. Sattel, K. Jung, H. Ehrhardt, V.S. Veerasamy, J. Robertson, Highly tetrahedral, diamond-like amorphous hydrogenated carbon prepared from a plasma beam source, Appl. Phys. Lett. 64 (1994) 2797–2799.
[38] A.J. Barthel, J. Luo, K.S. Hwang, J.-Y. Lee, S.H. Kim, Boundary lubrication effect of organic residue left on surface after evaporation of organic cleaning solvent, Wear 350–351 (2016) 21–26.
[39] A. Alazizi, A. Draskovics, G. Ramirez, A. Erdemir, S.H. Kim, Tribochemistry of Carbon Films in Oxygen and Humid Environments: Oxidative Wear and Galvanic Corrosion, Langmuir 32 (2016) 1996–2004.
[40] A. Fischer-Cripps, The Hertzian contact surface, J. Mater. Sci. 34 (1999) 129–137.
[41] S.B. Liu, A. Peyronnel, Q.J. Wang, L.M. Keer, An extension of the Hertz theory for three-dimensional coated bodies, Tribol. Lett. 18 (2005) 303–314.
[42] M. Kot, Contact mechanics of coating-substrate systems: Monolayer and multilayer coatings, Arch. Civil Mech. Eng. 12 (4) (2012) 464–470.
[43] Y.R. Jeng, S. Islam, K.T. Wu, A. Erdemir, O. Eryilmaz, Investigation of Nano-Mechanical and- Tribological Properties of Hydrogenated Diamond Like Carbon (DLC) Coatings, J. Mech. 33 (2016) 769–776.
[44] V.L. Popov, Contact mechanics and friction, Springer, 2010.
[45] X. He, Z. Liu, L.B. Ripley, V.L. Swensen, I.J. Griffin-Wiesner, B.R. Gulner, G. R. McAndrews, R.J. Wieser, B.P. Borovsky, Q.J. Wang, S.H. Kim, Empirical relationship between interfacial shear stress and contact pressure in micro- and macro-scale friction, Tribol. Int. 155 (2021) 106780, https://doi.org/10.1016/j.triboint.2020.106780.
[46] G. Amontons, De la Resistance Cause'e dans les Machines (1), J.-Japan. Soc. Tribolog. 44 (1999) 229–235.
[47] G.W. Thomson, The Antoine equation for vapor-pressure data, Chem. Rev. 38 (1946) 1–39.
[48] F. Mangolini, K.D. Koshigan, M.H. Van Benthem, J.A. Ohlhausen, J.B. McClimon, J. Hilbert, J. Fontaine, R.W. Carpick, How Hydrogen and Oxygen Vapor Affect the Tribochemistry of Silicon- and Oxygen-Containing Hydrogenated Amorphous Carbon under Low-Friction Conditions: A Study Combining X-ray Absorption Spectromicroscopy and Data Science Methods, ACS Appl. Mater. Interfaces 13 (2021) 12610–12621.

[49] F. Mangolini, J.B. McClimon, R.W. Carpick, Quantitative Evaluation of the Carbon Hybridization State by Near Edge X-ray Absorption Fine Structure Spectroscopy, Anal. Chem. 88 (2016) 2817–2824.
[50] F. Mangolini, F. Rose, J. Hilbert, R.W. Carpick, Thermally induced evolution of hydrogenated amorphous carbon, Appl. Phys. Lett. 103 (16) (2013) 161605, https://doi.org/10.1063/1.4826100.
[51] L.A. Langley, D.H. Fairbrother, Effect of wet chemical treatments on the distribution of surface oxides on carbonaceous materials, Carbon 45 (1) (2007) 47–54.
[52] K.A. Wepasnick, B.A. Smith, K.E. Schrote, H.K. Wilson, S.R. Diegelmann, D. H. Fairbrother, Surface and structural characterization of multi-walled carbon nanotubes following different oxidative treatments, Carbon 49 (1) (2011) 24–36.
[53] N. Mikhin, Calculation of coefficients of external friction and preliminary displacement, Friction, Wear and Lubrication, IV Kragelsky and VV Alisin, eds., Mir Publishers, Moscow, 1 (1978) 54–101.
[54] C.A. Coulomb, Théorie des machines simples en ayant égard au frottement de leurs parties et à la roideur des cordages, Bachelier, 1821.
[55] B. Derjaguin, Molekulartheorie der äußeren Reibung, Zeitschrift für Physik 88 (1934) 661–675.
[56] Z. Chen, X. He, C. Xiao, S. Kim, Effect of Humidity on Friction and Wear—A Critical Review, Lubricants 6 (3) (2018) 74, https://doi.org/10.3390/lubricants6030074.
[57] A.A. Al-Azizi, O. Eryilmaz, A. Erdemir, S.H. Kim, Effects of nanoscale surface texture and lubricant molecular structure on boundary lubrication in liquid, Langmuir 29 (2013) 13419–13426.
[58] S.E. Tomlinson, R. Lewis, M.J. Carré, The effect of normal force and roughness on friction in human finger contact, Wear 267 (2009) 1311–1318.
[59] C. Trevisiol, A. Jourani, S. Bouvier, Effect of hardness, microstructure, normal load and abrasive size on friction and on wear behaviour of 35NCD16 steel, Wear 388–389 (2017) 101–111.
[60] G.V. Lubarsky, M.R. Davidson, R.H. Bradley, Elastic modulus, oxidation depth and adhesion force of surface modified polystyrene studied by AFM and XPS, Surf. Sci. 558 (2004) 135–144.
[61] J. Gao, C. Xiao, C. Feng, L. Wu, B. Yu, L. Qian, S.H. Kim, Oxidation-induced changes of mechanochemical reactions at GaAs–SiO2 interface: The competitive roles of water adsorption, mechanical property, and oxidized structure, Appl. Surf. Sci. 548 (2021) 149205, https://doi.org/10.1016/j.apsusc.2021.149205.
[62] X.-W. Li, M.-W. Joe, A.-Y. Wang, K.-R. Lee, Stress reduction of diamond-like carbon by Si incorporation: A molecular dynamics study, Surf. Coat. Technol. 228 (2013) S190–S193.
[63] G. Jungnickel, T.h. Köhler, T.h. Frauenheim, M. Haase, P. Blaudeck, U. Stephan, Structure and chemical bonding in amorphous diamond, Diam. Relat. Mater. 5 (2) (1996) 175–185.
[64] A.R. Konicek, D.S. Grierson, A.V. Sumant, T.A. Friedmann, J.P. Sullivan, P.U.P. A. Gilbert, W.G. Sawyer, R.W. Carpick, Influence of surface passivation on the friction and wear behavior of ultrananocrystalline diamond and tetrahedral amorphous carbon thin films, Phys. Rev. B 85 (15) (2012), https://doi.org/10.1103/PhysRevB.85.155448.
[65] F. Mangolini, J.B. McClimon, F. Rose, R.W. Carpick, Accounting for nanometer-thick adventitious carbon contamination in X-ray absorption spectra of carbon-based materials, Anal Chem 86 (24) (2014) 12258–12265.
[66] G. He, M.H. Müser, M.O. Robbins, Adsorbed layers and the origin of static friction, Science 284 (1999) 1650–1652.
[67] H. Li, T. Xu, C. Wang, J. Chen, H. Zhou, H. Liu, Friction behaviors of hydrogenated diamond-like carbon film in different environment sliding against steel ball, Appl. Surf. Sci. 249 (2005) 257–265.
[68] P.L. Dickrell, W.G. Sawyer, A. Erdemir, Fractional Coverage Model for the Adsorption and Removal of Gas Species and Application to Superlow Friction Diamond-Like Carbon, J. Tribol. 126 (2004) 615–619.
[69] T.A. Blanchet, W.G. Sawyer, Differential application of wear models to fractional thin films, Wear 251 (2001) 1003–1008.
[70] Y.A. Wang, J.X. Li, Y. Yan, L.J. Qiao, Effect of surface film on sliding friction and wear of copper-impregnated metallized carbon against a Cu–Cr–Zr alloy, Appl. Surf. Sci. 258 (2012) 2362–2367.
[71] F. Guo, G. Dong, L. Dong, High temperature passive film on the surface of Co–Cr–Mo alloy and its tribological properties, Appl. Surf. Sci. 314 (2014) 777–785.
[72] X. Wu, T. Ohana, T. Nakamura, A. Tanaka, Gaseous Tribochemical Products of Hydrogenated DLC Film and Stainless Steel Pair in Air Detected by Mass Spectrometry, Tribol. Lett. 57 (1) (2015), https://doi.org/10.1007/s11249-014-0448-3.
[73] M.J. Marino, E. Hsiao, L.C. Bradley, O.L. Eryilmaz, A. Erdemir, S.H. Kim, Is Ultra-Low Friction Needed to Prevent Wear of Diamond-Like Carbon (DLC)? An Alcohol Vapor Lubrication Study for Stainless Steel/DLC Interface, Tribol. Lett. 42 (2011) 285–291.
[74] A. Erdemir, The role of hydrogen in tribological properties of diamond-like carbon films, Surf. Coat. Technol. 146 (2001) 292–297.
[75] Y. Liu, Y. Jiang, J. Sun, L. Wang, Y. Liu, L. Chen, B. Zhang, L. Qian, Durable superlubricity of hydrogenated diamond-like carbon film against different friction pairs depending on their interfacial interaction, Appl. Surf. Sci. 560 (2021) 150023, https://doi.org/10.1016/j.apsusc.2021.150023.
[76] L. Chen, Z. Chen, X. Tang, W. Yan, Z. Zhou, L. Qian, S.H. Kim, Friction at single-layer graphene step edges due to chemical and topographic interactions, Carbon 154 (2019) 67–73.
[77] J. Andersson, R. Erck, A. Erdemir, Friction of diamond-like carbon films in different atmospheres, Wear 254 (2003) 1070–1075.
[78] F. Gao, A. Erdemir, W.T. Tysoe, The Tribological Properties of Low-friction Hydrogenated Diamond-like Carbon Measured in Ultrahigh Vacuum, Tribol. Lett. 20 (2005) 221–227.
[79] J. Fontaine, C. Donnet, A. Grill, T. LeMogne, Tribochemistry between hydrogen and diamond-like carbon films, Surf. Coat. Technol. 146 (2001) 286–291.
[80] B.J. Hamrock, B.J. Schmid, B.O. Jacobson, Fundamentals of fluid film lubrication, CRC press, 2004.
[81] A. Böttcher, H. Niehus, Oxygen adsorbed on oxidized Ru (0001), Phys. Rev. B 60 (20) (1999) 14396–14404.
[82] A.J. Barthel, S.H. Kim, Lubrication by physisorbed molecules in equilibrium with vapor at ambient condition: effects of molecular structure and substrate chemistry, Langmuir 30 (22) (2014) 6469–6478.
[83] A.A. Al-Azizi, O. Eryilmaz, A. Erdemir, S.H. Kim, Nano-texture for a wear-resistant and near-frictionless diamond-like carbon, Carbon 73 (2014) 403–412.
[84] X. Dai, N. Sun, S.O. Nielsen, B.B. Stogin, J. Wang, S. Yang, T.-S. Wong, Hydrophilic directional slippery rough surfaces for water harvesting, Sci. Adv. 4 (2018) eaaq0919.
[85] I. Nayshevsky, Q. Xu, A.M. Lyons, Hydrophobic-Hydrophilic Surfaces Exhibiting Dropwise Condensation for Anti-Soiling Applications, IEEE J. Photovoltaics 9 (1) (2019) 302–307.
[86] R.N. Wenzel, Resistance of solid surfaces to wetting by water, Ind. Eng. Chem. 28 (1936) 988–994.
[87] S. Eliezer, Y. Eliezer, The fourth state of matter: an introduction to plasma science, CRC Press, 2001.
[88] J. Hagen, Industrial catalysis: a practical approach, John Wiley & Sons, 2015.
[89] H. Yoshida, K. Koizumi, M. Boero, M. Ehara, S. Misumi, A. Matsumoto, Y. Kuzuhara, T. Sato, J. Ohyama, M. Machida, High Turnover Frequency CO–NO Reactions over Rh Overlayer Catalysts: A Comparative Study Using Rh Nanoparticles, J. Phys. Chem. C 123 (2019) 6080–6089.
[90] P. Panagiotopoulou, Hydrogenation of CO 2 over supported noble metal catalysts, Appl. Catal. A 542 (2017) 63–70.
[91] C. Carosella, J. Comas, Oxygen sticking coefficients on clean (111) silicon surfaces, Surf. Sci. 15 (1969) 303–312.